Quantifying the Van der Waals Interactions in Layered PdSe₂ by Inelastic X-ray Scattering under Pressure

Bin Wei^{1,2+}, Qingan Cai³⁺, Ahmet Alata⁴, Peng Lv¹, Ayman H. Said⁴, Yabin Chen¹, Chen Li^{3,5*}, Jiawang Hong^{1*}

¹School of Aerospace Engineering, Beijing Institute of Technology, Beijing 100081, China

²Henan Key Laboratory of Materials on Deep-Earth Engineering, School of Materials Science and Engineering, Henan Polytechnic University, Jiaozuo 454000, China

³Mechanical Engineering, University of California, Riverside, Riverside, CA 92521, USA

⁴Advanced Photon Source, Argonne National Laboratory, Argonne, IL 60439, USA

⁵Materials Science and Engineering, University of California, Riverside, Riverside, CA 92521, USA

- + These authors contributed equally to this work.
- * Corresponding authors: chenli@ucr.edu; hongjw@bit.edu.cn

Abstract

Van der Waals (vdW) force, weakly holding the layers together in two-dimensional (2D) materials, plays a key role in various physical properties, such as superconductivity, ferromagnetism, and quantum Hall effect. Quantifying the vdW interactions, therefore, is essential for understanding the fundamental mechanisms of these novel properties. However, due to the difficulty of probing the interlayer forces directly, it is still challenging to quantify the vdW interactions. In this work, we quantified the vdW interactions by investigating the pressure-dependence of the acoustic phonons in layered palladium diselenide (PdSe₂). To our acknowledge, the evolution of the classical out-of-plane bending vibration mode (ZA) with pressure was characterized *for the first time*. Inelastic X-ray scattering technique with diamond anvil cell was used to acquire the pressure dependence of the ZA mode. The interlayer binding changes from the weak vdW force to the

covalent bond, while the orthorhombic structure of PdSe₂ evolves into a cubic one. The interlayer-related elastic constants (C_{33} and C_{44}) increase by 6 and 8 times from ambient pressure to 6 GPa, respectively. The interlayer shear force constant f_{shear} and the compression force constant f_{direct} increase by 6 and 3.5 times through phase transition, respectively. These results indicate that the interlayer vdW interactions increased dramatically with increasing pressure and the covalent bond takes over after phase transition. Our work not only quantifies the pressure-dependent ZA mode in 2D-materials, but also, more significantly, paves a new path to measure the vdW interactions in 2D-materials system.

I. INTRODUCTION

In two-dimensional (2D) layered materials, weak van der Waals (vdW) force holds together the neighboring atomic layers, while stronger covalent or ionic bond holds the atoms together in the layers, leading to the anisotropy of crystal structures. Many unique physical properties and applications, such as high temperature superconductivity [1], ferromagnetism [2], and anomalous lattice vibrations [3,4], have been reported to relate closely to the interlayer vdW interactions of 2D-layered materials [5,6,7,8]. Therefore, measuring and tuning the vdW interactions are essential in exploring the extraordinary properties in 2D-layered materials. To date, various methods have been attempted to quantify the vdW interactions: atomic force microscopy (AFM) measurement [9,10] Raman [11,12], and pressure enhanced band splitting [13]. However, due to the limited capability in measuring the force and potential between the neighboring atomic layers, more efficient and accurate quantification of vdW interactions is still in urgent need.

Due to the weak interlayer vdW interactions, the phonon dispersions of layered materials are extremely sensitive to pressure. The pressure-dependent elastic constants, which describe relationship between stress and strain in solids, can be extracted from the acoustic phonons by using the semi-continuum model [14,15]. As is known, out-of-plane atomic vibrations contribute to two out-of-plane phonon modes (one acoustic and one optical), called flexural modes. In the phonon dispersion spectrum of 2D-layered materials, the acoustic flexural mode, named ZA mode [16], is tightly related to the interlayer weak vdW interactions. Thus, probing the pressure-dependence of ZA phonon frequency could be used to obtain the pressure-dependence of elastic constants related to vdW forces. Accordingly, high-pressure inelastic X-ray scattering (IXS) experiment is much appropriate and expected to measure the pressure dependence of phonon modes on layered materials, especially of ZA mode.

Palladium diselenide (PdSe₂), one of the 2D-layered transition metal dichalcogenides family, has attracted ever-increasing interests recently. It shows promising applications due to its superconductivity [17], multiple phase transition [18], negative Poisson's ratio [19], photovoltaicity [20], and ferroelasticity [21]. PdSe₂ undergoes a phase transition from an orthorhombic structure (Pbca) with a square-planar of Pd atoms to a cubic structure ($Pa\bar{3}$) with an octahedral of Pd atoms when hydrostatic pressure (HP) reaching 6 GPa (Figure 1) [22,23]. The vdW force between layers increases and the layer spacing decreases gradually when increasing pressure before phase transition; the vdW force disappears and the neighboring layers are connected by the covalent bond after phase transition. Thus, such structural evolution of PdSe₂ provides a natural advantage to probe the evolution of vdW interactions.

Here, we report a new method to study the vdW interactions through the acoustic phonons measured by pressure-dependent IXS in layered PbSe₂. The pressure-dependent dispersions of ZA mode are measured at 0.36, 1.85, 3.7, and 6 GPa. Phase transition is observed when the hydrostatic pressure is increased to 6 GPa. The interlayer-related elastic constants (C_{33} and C_{44}) and force constants (f_{direct} and f_{shear}) all show linear relations with pressure up to 6 GPa. With increasing pressure, the interlayer interactions become stronger and are taken over by the covalent bond after phase transition.

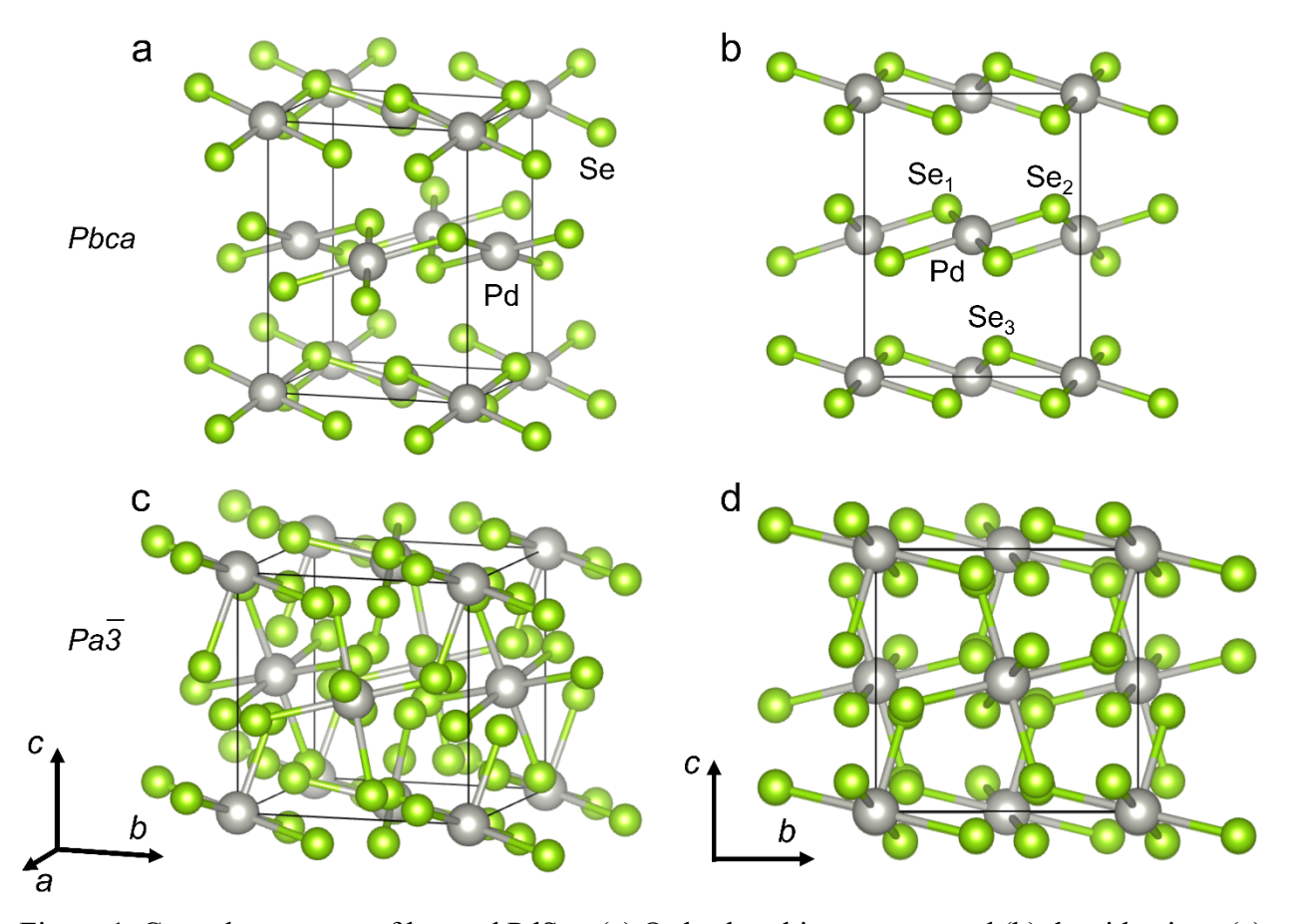


Figure 1. Crystal structures of layered PdSe₂. (a) Orthorhombic structure and (b) the side view. (c) Cubic structure and (d) the side view.

EXPERIMENT AND CALCULATION

High-pressure inelastic X-ray experiment

High quality 2D-layered PdSe₂ crystals in this work were grown by the chemical vapor transport method. The quality of crystals was checked by X-ray diffraction shown in Figure 2a. The full width at half maximum (FWHM) of X-ray diffraction peak at (002) plane is about $0.24 \pm 0.01^{\circ}$, showing high crystalline quality of the sample.

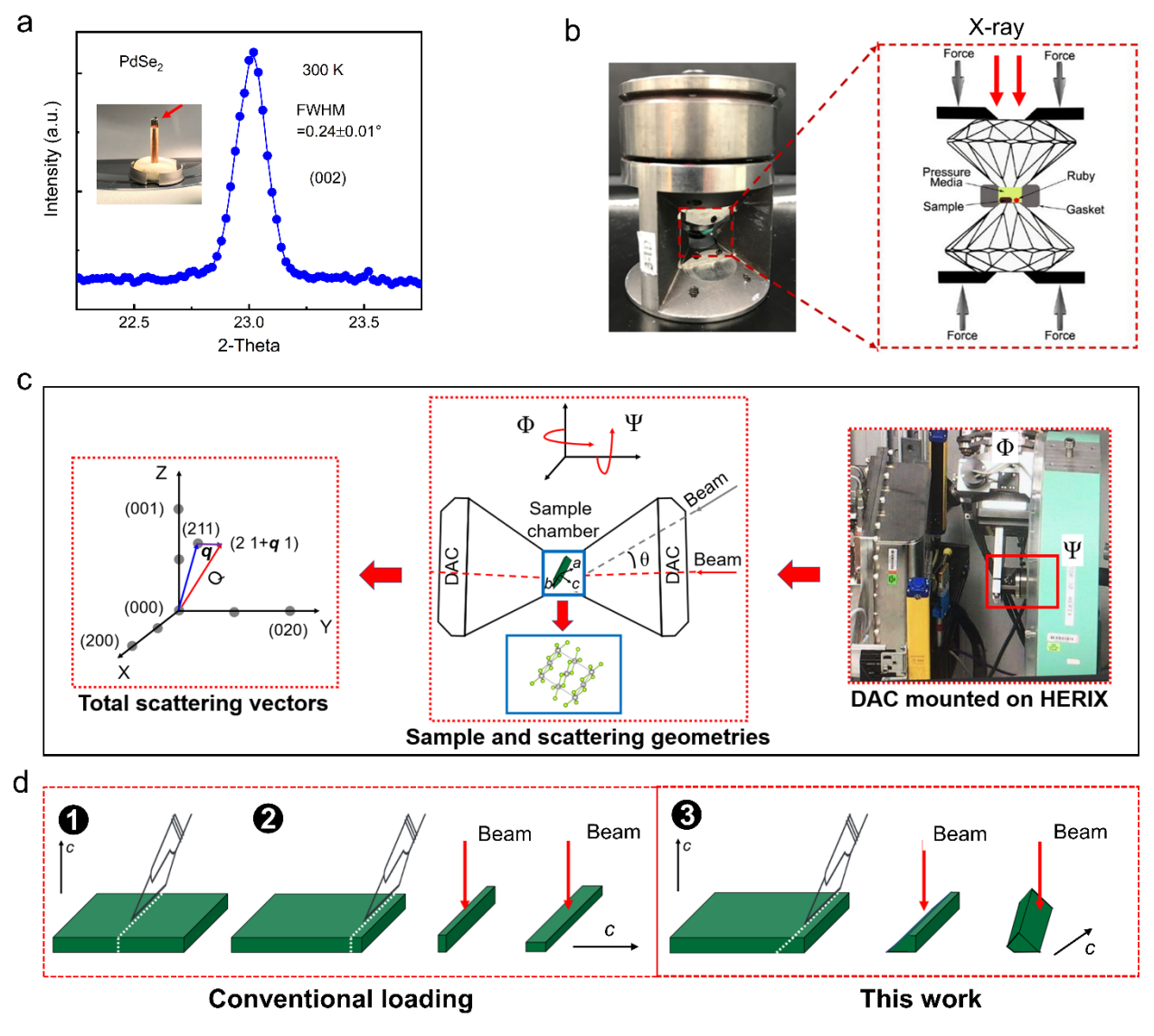


Figure 2. Sample preparation for pressure-dependent IXS measurement of layered PdSe₂ single crystal. (a) Rocking curve for (002) Bragg peak of PdSe₂ crystal. The narrow peak width (FWHM) shows high crystalline quality of the sample. Inset is the sample attached on a copper post for the ambient pressure measurement. (b) A small single crystal loaded in a panoramic DAC for high-

pressure measurement. (c) Schematic diagram of the beam scattering geometry for the high-pressure experiment. Red frame in the right panel shows the DAC mounted on HERIX. Middle panel shows the sample and beam scattering geometries for the high-pressure experiment. Left panel shows the scattering vectors in zone (211). (d) Sample geometry for ZA mode measurement under high pressure. 1 and 2 are commonly used for high-pressure IXS measurement, while 3 is the method used in this work.

High energy resolution inelastic X-ray scattering experiment was performed to measure the phonon dispersions of PdSe₂ layered crystal under ambient pressure, 0.36, 1.85, 3.7, and 6 GPa. The measurements were conducted at 30-ID-C (the High-resolution Inelastic X-ray Scattering beamline, HERIX) at Advanced Photon Source, Argonne National Laboratory [24,25]. Photon energy is 23.7 keV (wavelength at 0.5226 Å) and the beam is focused on a spot of $35 \times 5 \ \mu m^2$. The measurements were conducted at room temperature. For measurements under ambient pressure, the single crystal sample (2 mm × 1 mm × 60 μ m) was attached to a copper post by epoxy (inset in Figure 2a) and the post was mounted in the Huber 4-circle stage. Transmission scattering geometry was used to minimize the variation in scattering intensity due to the change of surface orientation between different Q points. The orientation matrix was defined by using Bragg peaks at (2 0 0), (0 2 0), and (0 0 2). Measured high symmetry directions in reciprocal space are along Γ -X, Γ -Y, and Γ -Z, respectively. At specific wave vector transfer (Q point), counting time at each energy step is $30 \sim 90$ s, which is adjusted by the phonon peak statistic.

For high pressure measurements, a small crystal (80 μ m \times 50 μ m \times 40 μ m) was loaded in a panoramic diamond anvil cell (DAC), and the DAC was aligned parallel to the electric field vectors of incident X-ray (Figure 2b). Culet size of DAC was 800 μ m, rhenium with thickness at 250 μ m was used as the gasket. The gasket was pre-indented to 120 μ m and a 400 μ m hole was drilled. Helium was used as the pressure medium to minimize the background and ensure the hydrostatic

pressure inside the chamber. Ruby fluorescence excited by 532 nm laser was used to measure the hydrostatic pressure. After gas loading, the initial pressure was 0.36 GPa, which was increased to 1.85, 3.7, and 6 GPa by step. Sample quality and the orientation matrix were checked before the measurements at each pressure. Figure 2(c) (right panel) shows the beam scattering geometry in HERIX for the high-pressure experiment. It can be seen that when the DAC was mounted on the roational stage, the incident beam angle is limited by the opening angle of DAC, the Φ angle of the roational stage is fixed, the Ψ angle has a certain degree of rotational freedom, and thus the scattering geometry is extremely limited. In order to measure the ZA mode, a Brillouin zone (BZ) with out-of-plane value and the q points along in-plane direction should be reached. Thus, if the single crystal sample is cut regularly as the first and second methods shown in Figure 2d and loaded lying on the diamond, there are two problems should be concerned: a) the obtained BZ only along one of the high-symmetry directions, which limits the rotation along the other direction; b) although the crystal is loaded along the right direction, it is difficult to keep the direction after He gas loading. In these cases, the scattering geometry and the rotation matrix can't satisfy the requirement for ZA measurement. Here, we use the third method in Figure 2d, where the sample is cut with a certain angle along an arbitrary direction between the c-axis. In this case, a crossplane BZ can be easier obtained, and the sample is more stable during gas loading, maintaining the scattering geometry the experiment. The $(2 \ 1+ \ q \ 1)$ zone was obtained for ZA mode measurement after He gas loading, and other phonons were also measured except for ZA according to dynamic structure factor $S(Q, \omega)$ simulation and IXS spectra. At specific wave vector transfer (Q point), counting time at each energy step is $60 \sim 120$ s. Due to the relative low statistics under high pressure, 3 or 5 scans were perfored at each Q points and the data are combined for analysis.

Phonon calculation

First-principles calculations were performed based on the density functional theory (DFT) as implemented in the Vienna Ab Initio Simulation Package (VASP) [26]. The generalized gradient approximation (GGA) Perdew-Burke-Ernzerhof (PBE) functional was used for structural relaxations with plane-wave cut-off energy of 600 eV. The optPBE functional [27] was used to estimate the vdW force due to layered structure PdSe₂ [28]. The BZ of the reciprocal space was sampled by a Γ -centered grid of 5 ×5 × 4. The force components of each atom were smaller than 0.001 eV/Å and the difference of total energy was less than 10^{-6} eV during the structure relaxation. The Phonopy code [29] was used to calculate the phonon dispersion of layered PdSe₂. In this approach, the second-order interatomic force constants (IFCs) were computed by the finite difference method in a 2 × 2 × 2 supercell. The lattice constants at each hydrostatic pressure were used from the measurements by HERIX.

III. RESULTS AND DISCUSSION

Phase transition under high pressure

Phase transition under high pressure is determined by tracking the variance of lattice constants. Due to the weak interlayer vdW force, the crystal structure is sensitive to pressure. Thus, before measuring the phonon dispersions, it is necessary to check the quality and confirm that the sample is intact under high pressure and after the phase transition. Due to the limited 2-theta angle by the opening angle of DAC, only several crystal planes on lower-order BZ can be observed (Figure S2). Figure 3a shows the X-ray Bragg diffraction (211) plane of PdSe₂ under each pressure, which is also presented from the diffraction patterns at 0.36 and 6 GPa It is found that each crystalline plane has a relatively sharp peak (Figure S2), indicating high quality of the sample and good agreement

with the predictions. The 2-theta shows an increase with increasing pressure before phase transition due to the reduced lattice constants. It drops to the minimum value under 6 GPa, indicating the phase transition from orthorhombic to cubic structure. Figure 3b shows that the inplane lattice constants a and b and unit cell volume V declines moderately with increasing pressure in orthorhombic phase, while the drop of out-of-plane lattice constant c is more significant due to the increasing of vdW interactions with pressure. The sharp drop of c and V indicates the structure transition from 3.7 (orthorhombic) to 6 GPa (cubic), also revealed by the increasing of the systematic free energy (Figure S1). The detailed diffraction and lattice information versus pressure can be found in Table SI. The ratios of a/c and b/c increase with the increasing pressure, indicating the compression along c and the structure evolution of PdSe₂. By fitting the trends of the lattice constants versus pressure from equation y=A+Bx+Cx², it is found that the decline rate of c (B=0.041, C=0.005) is larger than those of a (B=0.023, C=0.003) and b (B=0.026, C=0.003). This behavior reveals the negative Poisson's ratio in the orthorhombic structure of layered PdSe₂, which confirms the prediction in monolayer PdSe₂ [19] to some extent.

In addition, the energy integrated crystal orbital Hamiltonian population (ICOHP) was calculated corresponding to the Pd-Se bond lengths to evaluate the evolution of the bonding versus pressure, shown in Figure S3a and S3b. For Pd-Se₁ and Pd-Se₂, the bond lengths increase, and the bond strengths decrease gradually with the increasing pressure. While for Pd-Se₃, the bond length decreases, and the bond strength increase significantly with the increasing pressure. As reported, in orthorhombic structure, the low spin configuration $(z^2)^2(x^2-y^2)^0$ induces the square-planar [PdSe4] (composed by Pd-Se₁ and Pd-Se₂), while in cubic structure, the high spin configuration $(z^2)^1(x^2-y^2)^1$ induces the octahedral [PdSe6] (composed by Pd-Se₁, Pd-Se₂, and Pd-Se₃ in orthorhombic structure) [17,22]. This Jahn-Teller distortion of the octahedral [PdSe6], illustrated

in Figure S3d, will lead to weaker in-plane and stronger out-of-plane Pd-Se bonding at 6 GPa than below 6 GPa [30,31].

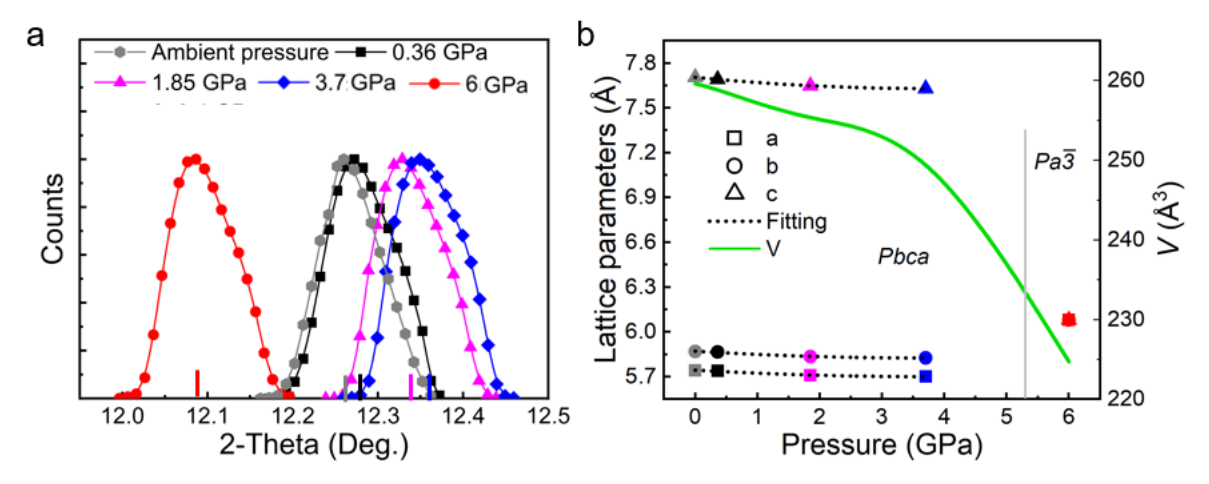


Figure 3. Pressure-dependent crystal change of PdSe₂. (a) Bragg peak of (211) plane by HERIX. The vertical solid lines are the predictions from DFT calculations. (b) Pressure-dependent lattice constants and the volume. Dot lines are the fitting curves from $y=A+Bx+Cx^2$. Green curve is guide for eyes. Vertical grey line represents the pressure of phase transition.

Pressure dependence of ZA mode

The lattice constants of PdSe₂ are sensitive to the pressure, so phonon dispersions will change with pressure as well (). As shown in Figures 4a-4c, the pressure-dependent acoustic phonon dispersions along Γ –Y direction, especially the ZA mode, were obtained by IXS (see the calculated phonon dispersions of PdSe₂ under each pressure in Figure S4). It can be found that our first-principles calculations show excellent agreement with the measurements for the longitudinal acoustic (LA) and transverse acoustic (TA) phonons, while it is unable to predict the pressure dependence of ZA phonons. This discrepancy may results from the pressure dependent vdW interactions which may not be accurately described by the optPBE functional, though it shows good accuracy to estimate

the lattice constant at ambient condition [28]. For LA and TA modes, it is found that the phonon branches stiffen with the increasing pressure below 6 GPa and drop down at 6 GPa. For the ZA mode, the branch keeps stiffening as the pressure increases. Such difference results from the evolution of the lattice constants with pressure. In-plane lattice constants a and b decrease continuously before phase transition and increase significantly after that, while c keeps decreasing with the increasing pressure. Thus, the force constants between the heavier atoms Pd (Pd: 106.4 >Se: 78.97), which dominated the phonon energy around BZ center [33], increase gradually along a- and b-axis below 6 GPa and drop down at 6 GPa, while they keep increasing along c-axis with the increasing pressure (Figure S3c).

To our knowledge, it is the first experiment to measure the ZA dispersion curves with pressure dependence in 2D-layered materials. Due to the failure of first-principles calculations in estimating the pressure-dependent phonon energy in ZA mode, the exponential function, $\omega = \alpha q^{\beta}$, is applied to fit the measured phonon energy of ZA [34], showing the excellent agreement. As shown in Figures 4d and 4e, with increasing pressure, the ZA dispersion curve evolves toward linear gradually and the exponential coefficient decreases from 1.35 to 1. As is known, the dispersion curve exhibits a parabolic behavior in pure 2D materials, and β is smaller than 2 in the bulk layered single crystal. After phase transition, the dispersion curve is linear ($\beta = 1$). The change of β indicates that the interlayer vdW force increases gradually with the increasing pressure and is taken over by the covalent bond after phase transition.

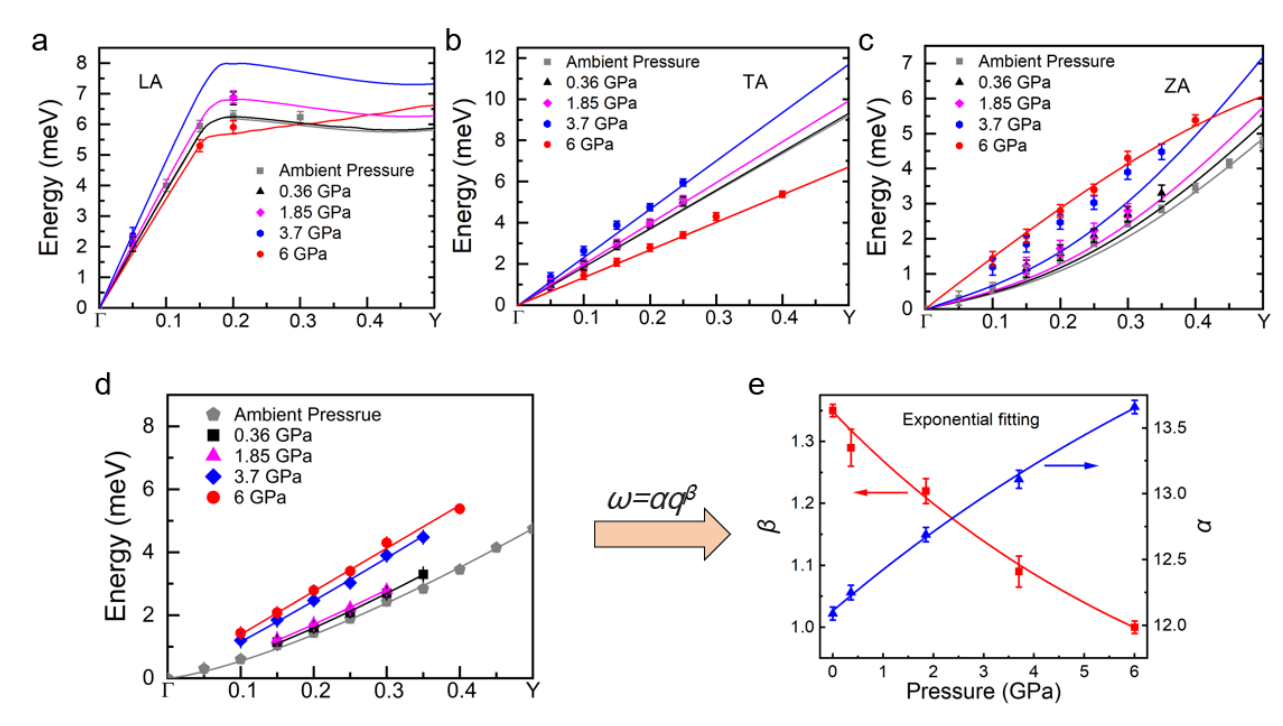


Figure 4. Pressure-dependent acoustic phonon dispersions along Γ -Y of PdSe₂. (a)-(c) Measured phonon modes of LA, TA, and ZA branches (symbols), overlaid with the corresponding first-principles calculations (Lines). (d) Exponential fittings of the ZA branches with ω = αq^{β} function (arrow). (e) Pressure-dependent fitting parameters α and β . Error bars are the fitting uncertainty.

Quantifying the vdW interactions

The elastic constant, representing the stress-strain relationship in materials, is highly sensitive to the pressure. The vdW interactions can be quantified through their corresponding elastic constants. The pressure-dependent elastic constants can be extracted from the acoustic phonons by using the semi-continuum model [35,]:

$$v_{\text{LA}(\Gamma-Y)} = \frac{\omega}{q} = \sqrt{\frac{C_{22}}{\rho}}, v_{\text{LA}(\Gamma-Z)} = \frac{\omega}{q} = \sqrt{\frac{C_{33}}{\rho}}, v_{\text{TA}(\Gamma-Y)} = \frac{\omega}{q} = \sqrt{\frac{C_{66}}{\rho}}$$
(1)

where v is the phonon group velocity near BZ center, ω the phonon energy, ρ the mass density and q the wavevector. For the ZA mode, we can obtain both C_{44} and the bending elastic parameter b_y by fitting the ZA dispersion from the following equation [37] (Figure S5):

$$\omega^2 = \frac{C_{44}}{\rho} q^2 + b_y^2 q^4 \tag{2}$$

 b_y represents the resistance of a layer to bend. The detailed fitted group velocities from the IXS data and the elastic constants are shown in Table SII-SIV and plotted in Fig. 5. C_{22} is associated with the compression vibration along b-axis, corresponding to LA mode along Γ -Y and the change of the lattice parameter b, while C_{66} is associated with the shear vibration along the in-plane direction, corresponding to the change of in-plane lattice parameters a and b. Below 6 GPa, C_{22} and C_{66} both show linear relation with pressure and increase by 50% near the phase transition; at 6 GPa, C_{22} and C_{66} both drop down to a lower value than that at ambient pressure. Such behavior is mainly attributed to the much larger in-plane lattice parameters in cubic structure.

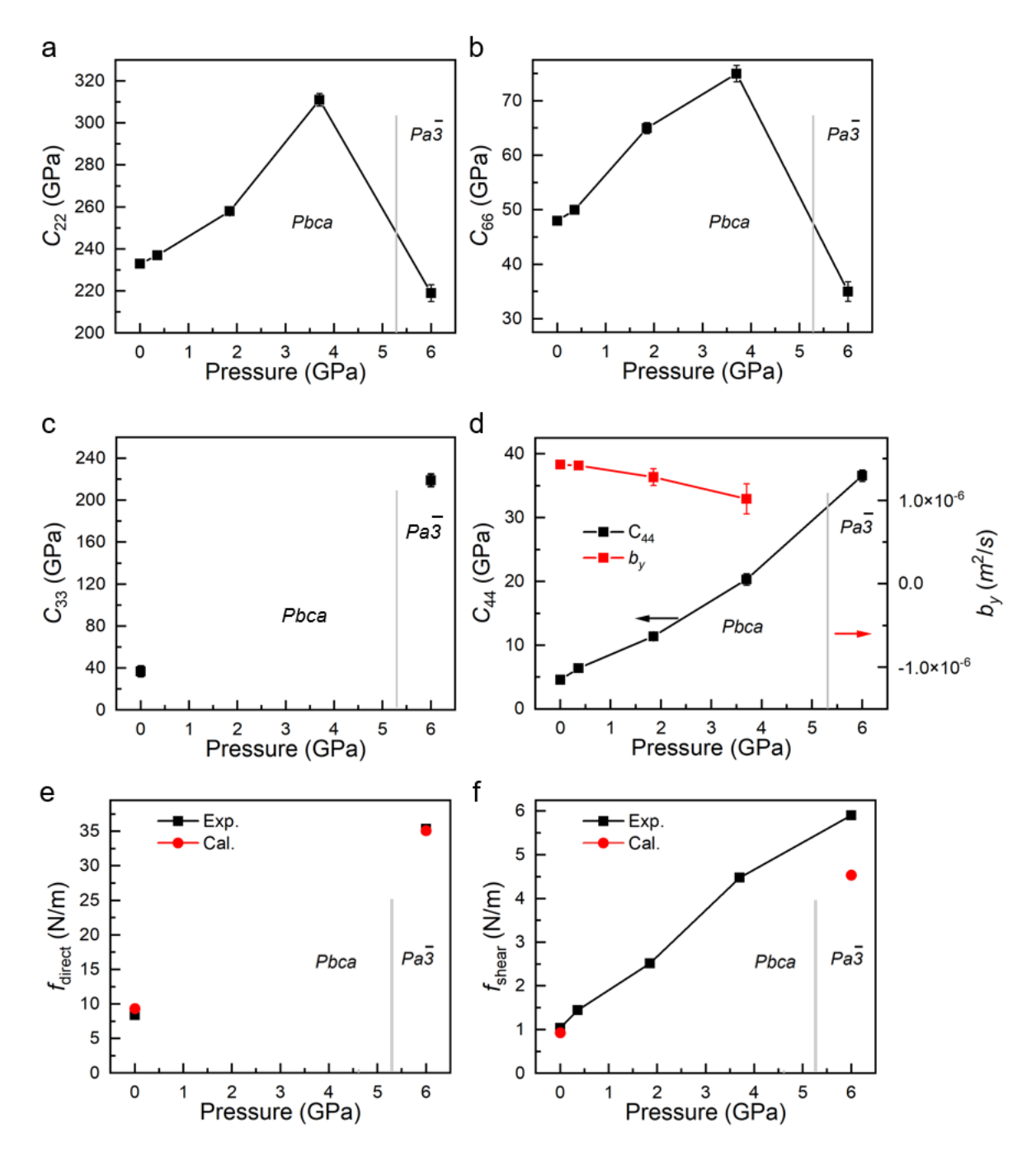


Figure 5. Pressure-dependent elastic constants of PdSe₂. (a) C_{22} , (b) C_{66} , (c) C_{33} , (d) C_{44} and b_y . Interlayer compression and shear force constants are respectively shown in (e) and (f). Error bars are the fitting uncertainty. The grey lines indicate the phase transition pressure.

 C_{33} is associated with the compression vibration along c-axis, corresponding to the LA mode along Γ -Z and the change of the lattice parameter c. It is a direct evaluation of the change of vdW

interactions between layers. Due to the beam scattering limitation and the ambiguous resolution to distinguish the extremely low energy of the LA mode along Γ –Z, we only obtain C_{33} under the ambient pressure and 6 GPa. As shown in Figure 5c, C_{33} is much smaller than C_{22} under ambient pressure due to the weak vdW force between layers. With increasing pressure, C₃₃ increases dramatically and the value in cubic structure (equivalent to C_{22}) is 6 times higher than that in orthorhombic structure, indicating the continuous increase of the interlayer force. C₄₄ represents the shear vibration where the atoms vibrate along c direction and vibrational wave propagates along Γ -Y, corresponding to the ZA mode along Γ -Y and the change of the lattice parameters b and c. C₄₄ shows the lowest value among the elastic constants because of the interlayer shear vibration affected by the weak vdW force, as shown in Figure 5. With the decreasing layer distance and the increasing ratio of b/c, the shear stress will increase significantly and lead to a linear relationship with pressure (Figure 5d). Under 6 GPa, C_{44} (equivalent to C_{66}) shows seven times higher than that at ambient pressure. Due to the bulk single crystal of PdSe₂ used in this work where the vdW force is stronger than that in monolayer materials, b_y is 1.43×10^{-6} m²/s at ambient pressure and is five times higher than that of single layer graphene (0.313 $\times 10^{-6}$ m²/s) [40]. With the pressure increased, during the bending on PdSe₂, the intralayer tension or compression and interlayer shear behaviors will both emerge and compete with each other. b_{ν} decreases slightly with increasing pressure, resulting from the increasing shear effect between layers. Compared with C_{22} and C_{66} , the interlayer related C_{33} and C_{44} increases faster with pressure (C_{22} and C_{66} increase by about 50% near the phase transition, while C_{33} and C_{44} increase by 6 and 7 times, respectively).

The interlayer compression (f_{direct}) and shear (f_{shear}) force constants can be used to evaluate the interlayer interactions with the layer spacing (c), expressed as: $f_{\text{direct}} = c \cdot C_{33}$ and $f_{\text{shear}} = c \cdot C_{44}$ [42].

In Figs. 5(e) and 5(f), our first-principles calculations show good agreement with the experiments. The layer spacing decreases gradually with increasing pressure, shown in Table SV. f_{direct} changes from about 10 N/m to about 35 N/m before and after phase transition, increased by 2.5 times, while f_{shear} shows a linear relation with pressure, which changes from 1 N/m to 6 N/m, increased by 5 times. These behaviors are mainly due to the enhancement of vdW force between layers, which provide an effective reflection on the evolution of vdW interactions with the layer distance.

CONCLUSION

In this work, the vdW interactions of layered PdSe₂ were studied by the combination of highpressure inelastic X-ray scattering and first-principles calculations. The pressure-induced phase transition was confirmed and the pressure-dependent acoustic phonon dispersions along Γ –Y direction were measured. The lattice structure of PdSe₂ transfers from the orthorhombic phase to cubic phase and the interlayer vdW force disappears from 3.37 GPa to 6 GPa. Below 6 GPa, C_{22} , C_{33} , C_{44} and C_{66} increase linearly with increasing pressure. b_y decreases with increasing pressure due to the enhancement of the interlayer shear effect when the competition between the intralayer tension or compression with the interlayer shear effect. The interlayer shear force constant f_{shear} and the compression force constant f_{direct} increase with increasing pressure, indicating the enhancement of the interlayer vdW interactions.

Our experimental results show that with the change of pressure, the interlayer compression (f_{direct}) and shear (f_{shear}) force constants reflect the evolution of interlayer vdW interactions with pressure. Our work confirmed that the high-pressure IXS measurement is effective to characterize the interlayer vdW interaction. It should be noted that the sample need to be loaded in a special orientation to satisfy the required scattering geometry of high-pressure IXS measurement to

directly measure the interlayer vdW interactions. In addition, due to the weak interaction between layers, the acoustic phonons along Γ –Z localize in the low energy region, a spectrometer with higher resolution is thus needed to distinguish these phonon modes. However, although the sample loading and the instrument setup are still challenging, with the development of experimental technology, high-pressure IXS will be more effective to characterize the vdW interaction. Our work is not only expected to measure other 2D-materials, but also paves a new path to characterize the vdW interactions.

AUTHOR CONTRIBUTIONS: J.H. conceived this project. B.W., Q.C., A.A. and Y.C. designed the experiments. B.W., Q.C., A.A. A.H.S., and C.L. performed the high-pressure inelastic X-ray scattering measurements. B.W. and P.L. performed the theoretical calculation. B.W., Q.C., J.H., and C.L. discussed the data. B.W., Q.C., J.H. and C.L. wrote the manuscript. All authors contributed to discussing the data and editing the manuscript.

COMPETING INTEREST STATEMENT: The authors declare no conflict of interest.

ACKNOWLEDGEMENT

The work at Beijing Institute of Technology is supported by the National Natural Science Foundation of China with Grant No. 11572040 and Beijing Natural Science Foundation (Grant No. Z190011). This work is supported by University of California, Riverside via Initial Complement. Inelastic X-ray scattering measurements used resource at Advanced Photon Source (APS), a Department of Energy (DOE) Office of Science User Facility operated by Argonne National Laboratory (ANL).

Reference:

1

- ⁷ T. Cheng, H. Lang, Z. Li, Z. Liu, and Z. Liu, "Anisotropic carrier mobility in two-dimensional materials with tilted Dirac cones: theory and application," *Phys. Chem. Chem. Phys.*, vol. 19, no. 35, pp. 23942–23950, 2017
- ⁸ L. Li *et al.*, "Emerging in-plane anisotropic two-dimensional materials," *InfoMat*, vol. 1, no. 1, pp. 54–73, Mar. 2019,

¹ Dean C R, Young A F, Meric I, et al. Boron nitride substrates for high-quality graphene electronics[J]. Nature Nanotechnology, 2010, 5(10): 722-726.

² T. Kimura and Y. Tokura, "Layered Magnetic Manganites," *Annual Review of Materials Science*, vol. 30, no. 1, pp. 451–474, 2000,

³ A. Splendiani *et al.*, "Emerging Photoluminescence in Monolayer MoS ₂," *Nano Lett.*, vol. 10, no. 4, pp. 1271–1275, Apr. 2010,

⁴ C. Lee, H. Yan, L. E. Brus, T. F. Heinz, J. Hone, and S. Ryu, "Anomalous Lattice Vibrations of Single- and Few-Layer MoS ₂," *ACS Nano*, vol. 4, no. 5, pp. 2695–2700, May 2010,

⁵ J. Wan, S. D. Lacey, J. Dai, W. Bao, M. S. Fuhrer, and L. Hu, "Tuning two-dimensional nanomaterials by intercalation: materials, properties and applications," *Chem. Soc. Rev.*, vol. 45, no. 24, pp. 6742–6765, 2016.

⁶ P. Zhang, F. Wang, M. Yu, X. Zhuang, and X. Feng, "Two-dimensional materials for miniaturized energy storage devices: from individual devices to smart integrated systems," *Chem. Soc. Rev.*, vol. 47, no. 19, pp. 7426–7451, 2018

⁹ Ternes M, González C, Lutz C P, et al. Interplay of conductance, force, and structural change in metallic point contacts[J]. Physical Review Letters, 2011, 106(1): 016802.

¹⁰ Liu, K.; Yan, Q.; Chen, M.; Fan, W.; Sun, Y.; Suh, J.; Fu, D.; Lee, S.; Zhou, J.; Tongay, S. Nano Lett. 2014, 14 (9), 5097–5103.

¹¹ S. Kawai *et al.*, "Van der Waals interactions and the limits of isolated atom models at interfaces," *Nat Commun*, vol. 7, no. 1, p. 11559, Sep. 2016,

¹² Aradhya, S. V.; Frei, M.; Hybertsen, M. S.; Venkataraman, L. Nat. Mater. 2012, 11 (10), 872–876.

¹³ P. Ci *et al.*, "Quantifying van der Waals Interactions in Layered Transition Metal Dichalcogenides from Pressure-Enhanced Valence Band Splitting," *Nano Lett.*, vol. 17, no. 8, pp. 4982–4988, Aug. 2017,

¹⁴ Nihira T and Iwata T 2003 Temperature dependence of lattice vibrations and analysis of the specific heat of graphite Phys. Rev. B 68 134305

¹⁵ Komatsu K and Nagamiya T 1951 Theory of specific heat of graphite J. Phys. Soc. Japan 6 438-44

¹⁶ J.-W. Jiang, B.-S. Wang, J.-S. Wang, and H. S. Park, "A review on the flexural mode of graphene: lattice dynamics, thermal conduction, thermal expansion, elasticity and nanomechanical resonance," *J. Phys.: Condens. Matter*, vol. 27, no. 8, p. 083001, Mar. 2015,

¹⁷ M. A. ElGhazali *et al.*, "Pressure-induced superconductivity up to 13.1 K in the pyrite phase of palladium diselenide PdS e 2," *Phys. Rev. B*, vol. 96, no. 6, p. 060509, Aug. 2017,

¹⁸ S. Bordier, A. Chocard, and S. Gossé, "Thermodynamic assessment of the palladium–selenium (Pd–Se) system," *Journal of Nuclear Materials*, vol. 451, no. 1–3, pp. 120–129, Aug. 2014,

¹⁹ Liu G, Zeng Q, Zhu P, et al. Negative Poisson's ratio in monolayer PdSe2[J]. Computational Materials Science, 2019, 160: 309-314.

²⁰ W. Lei *et al.*, "A new 2D high-pressure phase of PdSe ₂ with high-mobility transport anisotropy for photovoltaic applications," *J. Mater. Chem. C*, vol. 7, no. 7, pp. 2096–2105, 2019,

²¹ W. Lei *et al.*, "Ferroelastic lattice rotation and band-gap engineering in quasi 2D layered-structure PdSe ₂ under uniaxial stress," *Nanoscale*, vol. 11, no. 25, pp. 12317–12325, 2019,

²² Experimental and Theoretical Investigation on the Relative Stability of the PdS2and Pyrite mil ype Structures of PdSe2[J]. ChemInform, 2004, 35(25).

- ²⁵ A. H. Said, H. Sinn, R. Divan. New developments in fabrication of high-energy resolution analyzers for inelastic X-ray spectroscopy. J. Synchrotron Radiat. 18, 492-496 (2011).
- [26] Kresse, G. & Furthmüller, J. Efficiency of ab-initio total energy calculations for metals and semiconductors using a plane-wave basis set. Phys. Rev. B 54, 11169 (1996); Comput. Mater. Sci. 6, 15-50 (1996).
- [27] J. Klimeš, D. R. Bowler, and A. Michaelides, Chemical accuracy for the van der waals density functional, J. Phys.: Condens. Matter 22, 022201 (2009).
- ²⁸ Lv, P., Tang, G., Liu, Y., Lun, Y., Wang, X., & Hong, J. (2021). Van der Waals direction transformation induced by shear strain in layered PdSe2. Extreme Mechanics Letters, 101231.
- [29] Togo, A., Oba, F. & Tanaka, I. First-principles calculations of the ferroelastic transition between rutile-type and -type at high pressures. Phys. Rev. B 78, 134106 (2008).
- ³⁰ Kugel K I, Khomskii D I. The Jahn-Teller effect and magnetism: transition metal compounds[J]. Soviet Physics Uspekhi, 1982, 25(4): 231
- ³¹ Whangbo M H, Koo H J. Orbital interaction analysis of cooperative Jahn–Teller distortion, orbital ordering, spin ordering, and spin exchange interactions in magnetic solids[J]. Solid State Sciences, 2002, 4(3): 335-346.
- ³³ Christensen, M., Abrahamsen, A. B., Christensen, N. B., Juranyi, F., Andersen, N. H., Lefmann, K., ... & Iversen, B. B. (2008). Avoided crossing of rattler modes in thermoelectric materials. Nature materials, 7(10), 811-815.
- ³⁴ Jiang J W , Wang J S . A universal exponential factor in the dimensional crossover from graphene to graphite[J]. Journal of Applied Physics, 2010, 108(12):555.
- ³⁵ Nihira T and Iwata T 2003 Temperature dependence of lattice vibrations and analysis of the specific heat of graphite Phys. Rev. B 68 134305
- ³⁷ Komatsu K and Nagamiya T 1951 Theory of specific heat of graphite J. Phys. Soc. Japan 6 438–44
- ⁴⁰ Nihira T, Iwata T. Temperature dependence of lattice vibrations and analysis of the specific heat of graphite[J]. Physical Review B, 2003, 68(13): 134305.
- ⁴¹ Wang G, Dai Z, Xiao J, et al. Bending of Multilayer van der Waals Materials[J]. Physical Review Letters, 2019, 123(11): 116101.
- ⁴² Zabel H, Kamitakahara W A, Nicklow R M. Neutron scattering investigation of layer-bending modes in alkali-metal—graphite intercalation compounds[J]. Physical Review B, 1982, 26(10): 5919.

²³ Elghazali M A , Naumov P G , Mirhosseini H , et al. Pressure-induced superconductivity up to 13.1 K in the pyrite phase of palladium diselenide PdSe2[J]. Physical Review B, 2017.

²⁴ T. Toellner, A. Alatas, A. Said. Six-reflection meV-monochromator for synchrotron radiation. J. Synchrotron Radiat. 18 (2011) 605-611.